RSC Advances

PAPER

View Article Online
View Journal | View Issue

Cite this: *RSC Adv.*, 2017, **7**, 41004

Crystallinity of regenerated cellulose from [Bmim]Cl dependent on the hydrogen bond acidity/basicity of anti-solvents†

Zhaosheng Fan,[a] Jianbo Chen,[b] Wenji Guo,[a] Fang Ma,[a] Suqin Sun[a] and Qun Zhou *[a]

Received 25th July 2017
Accepted 14th August 2017

DOI: 10.1039/c7ra08178b

rsc.li/rsc-advances

Cellulose, regarded as a potential sustainable resource for the future, can dissolve and regenerate in ionic liquids (ILs) upon adding anti-solvents. Improving the regeneration conditions, like changing the anti-solvents, could optimize the properties of regenerated cellulose-based materials. Previous studies pointed out that the diffusion processes of anti-solvents plays a significant role in the determination of the properties of regenerated cellulose fibers/films. However, the cellulose regeneration mechanism from ILs has not been clarified. Here, attenuated total reflection Fourier transform infrared (ATR-FTIR) spectroscopy was introduced to monitor the molecular diffusion processes of four anti-solvents *in situ*. The crystallinity of regenerated cellulose showed a negative correlation with respect to the diffusion coefficient. In addition, the interaction of imidazolium cations and anti-solvent molecules was evaluated from the peak shifting during the diffusion processes. Furthermore, Taft and Kamlet scales were used to quantify the interaction between IL cations/anions and anti-solvent molecules, eliciting distinct cellulose regeneration paths in different anti-solvents.

1 Introduction

Since biomass energy production and consumption have comprised nearly 50% of the total renewable sources of energy in the United States in the last two decades, biorenewable resources are one of the promising alternatives for the looming depletion of fossil resources.[1] Much attention has been focused on the utilization of biomass directly or after conversion for a long time. Since cellulose is the most abundant biomass around the world,[2] a large amount of research on cellulose dissolution in ILs has been conducted since 2002. ILs refer to fluids comprised entirely by ions at room temperature, and have the advantages of negligible vapor pressure, low melting point, general non-flammability, thermal stability over a wide range of temperatures and simple recycling, among others.[3,4] In particular, ILs can be reused after removing the dissolved cellulose and anti-solvents.[5,6] During the last few years, the mechanism of cellulose and wood dissolving in ILs has been extensively and thoroughly studied.[7–9] After dissolving, cellulose can be degraded to potential sustainable resources of fuel or chemicals through chemical[10] or biological[11] strategies. Otherwise, cellulose can be regenerated to fabricate cellulose-based materials[12] with excellent properties by adding anti-solvents such as water, acetone and compressed carbon dioxide.[13] It is important to point out that the properties of regenerated cellulose varied upon changing the regeneration conditions.[14] The properties of cellulose-based materials may be optimized by adjusting the regeneration conditions such as changing the anti-solvents.[15] However, there has been far less research on cellulose regeneration from IL solutions than cellulose dissolution.[16] It has been reported that the diffusion rates of the cellulose solvent determined the mechanical properties of regenerated cellulose films from NaOH/urea solution.[17] Moreover, the initial modulus of the cellulose fiber as well as the fiber cross-sectional shapes were profoundly influenced by the diffusion rates of both the cellulose solvent-NH_3/NH_4SCN and anti-solvents.[18] In addition, cellulose fibers and films were also regenerated from an *N*-methylmorpholine-*N*-oxide solution using alcohols with different alkyl groups and water. Compared with water, alcohols are softer anti-solvents. Therefore, the morphology of the regenerated cellulose fibers and films exhibited an increasing regularity as the length of the alkyl chains shortened. In addition, the mechanical properties of these regenerated cellulose fibers and films decreased with the same trend.[19] Nevertheless, the mechanism of the regular change has not been discussed and verified further.

ATR-FTIR has been extensively used to monitor diffusion processes.[20–22] In this work, the diffusion processes of anti-solvents into cellulose solutions were monitored *in situ* using ATR-FTIR, revealing that the crystallinity of regenerated cellulose gel was significantly impacted by the anti-solvent diffusion

[a]*Department of Chemistry, Key Laboratory of Bioorganic Phosphorus Chemistry & Chemical Biology (Ministry of Education), Tsinghua University, Beijing 100084, China. E-mail: zhouqun@mail.tsinghua.edu.cn*

[b]*School of Life Sciences, Beijing University of Chinese Medicine, Beijing 100029, China*

† Electronic supplementary information (ESI) available. See DOI: 10.1039/c7ra08178b

coefficients. The anti-solvent diffusion coefficients were determined by the interaction between the anti-solvents and IL ions. According to the peak shift, we evaluated the interaction of imidazolium cation–anti-solvent complexes. We also proposed charge transfer models of imidazolium cation–anti-solvent complexes by multi-peak shifts. Through Taft and Kamlet scales, we analyzed the hydrogen bond (HB) acidity/basicity of each anti-solvent, suggesting that the HB acidity/basicity of the anti-solvents determines their molecular diffusion coefficients and impacts the crystallinity of regenerated cellulose. Furthermore, the Taft and Kamlet scales showed that the main driving forces of the anti-solvents differ from each other, indicating that there are various cellulose regeneration paths.

2 Experimental

2.1 Chemicals

An ionic liquid, 1-butyl-3-methylimidazolium chloride ([Bmim]Cl, ≥99%), was purchased from Shanghai Macklin Biochemical Co., Ltd and used without any pretreatment. Micro-crystalized cellulose (MCC) and silver nitrate were purchased from Sinopharm Chemical Reagents Co. Ltd. Methanol, ethanol and *n*-propanol were all purchased from Tianjin Kemiou Chemical Reagent Co. Ltd. (Tianjin City, China). Deionized water was homemade in the laboratory.

2.2 Cellulose dissolution and reassembly

MCC was added into [Bmim]Cl (1 : 20, w/w) in a 25 mL round-bottomed flask, and heated in an oil bath at 110 °C with magnetic stirring at *ca.* 300 rpm for two hours. Afterwards, a faint yellow homogeneous cellulose solution was obtained. Approximately 1 mL of the cellulose solution was poured into a 10 mL beaker and 9 mL of anti-solvent was then added. The anti-solvent diffused into the cellulose solution and [Bmim]Cl penetrated into the anti-solvent at room temperature. The anti-solvent was replaced a few times with equivalent fresh anti-solvent until the chloride ions in the cellulose gel were washed out. The chloride ions were detected by aqueous silver nitrate.

2.3 Characterization of the cellulose gel

X-ray diffraction (XRD). The XRD patterns with Cu Kα radiation ($\lambda = 1.5406$ Å) operated at 40 kV and 40 mA were recorded in the range of $2\theta = 5$–$60°$ with an XRD diffractometer (Bruker D8 Advance, Germany).

Cross-polarization magic angle spinning carbon nuclear magnetic resonance (^{13}C CP MAS NMR). ^{13}C CP MAS NMR spectra were recorded on a JEOL JNM-ECZ600R/M1 spectrometer (Japan) with a static field strength of 14 T (600 MHz) at ambient temperature. The contact time for CP was 2 ms with a proton pulse of 0.1 μs, and 1474 scans were accumulated. The MAS speed was 12 kHz. The delay time after the acquisition of the FID signal was 2 s.

Scanning electron microscopy (SEM). The cellulose gels were dried using supercritical carbon dioxide to retain the original network of the cellulose gels. Water, methanol and *n*-propanol were exchanged by ethanol when conducting the supercritical carbon dioxide drying. Before taking the images, a thin film of gold was sputtered over the cellulose aerogels for better observation using a Hitachi (Japan) model SU-8010 scanning electron microscope.

2.4 Diffusion test

The diffusion test was executed with a FTIR spectrometer (PerkinElmer, MA, USA) with a general ATR sampling accessory (PerkinElmer, MA, USA) attached. The diamond/ZnSe trapezoidal inner reflection element ATR crystal has a refractive index of 2.417. The incidence angle is 45°, giving three reflections in contact with the sample. The spectra were measured at 4 cm^{-1} resolution with 16 scans taking about 86 seconds. The wavenumber range was from 4000 to 650 cm^{-1}. A hollow stainless steel tube with a diameter of 10 millimeters was placed on the stage of the ATR accessory (Fig. 1). 100 microliters of hot cellulose solution was added into the tube and freely spread evenly over the diamond/ZnSe crystal. After cooling to ambient room temperature, 1 mL of anti-solvent was slowly injected into the tube. Meanwhile, the FTIR spectrometer started collecting data continuously using the Timebase software.

3 Results and discussion

3.1 Characterization of the regenerated cellulose

Notably, the diffraction peak of the hydrogel is characteristic for amorphous cellulose, while the peaks of the ethanol/*n*-propanol gel are for crystallized cellulose (Fig. 2a).[23] The diffraction peaks become increasingly intensive and narrow in the order water < methanol < ethanol < *n*-propanol, indicating that the crystallinity of the regenerated cellulose increased in the same order. In the ^{13}C CP MAS NMR spectra, the peak at 75.6 ppm gradually becomes sharp in the opposite sequence (Fig. 2b). Considering that the peak at ~75.6 ppm is characteristic for C2,3,5 attached by cellulose hydroxyl groups, variation of the HB network in cellulose could have an effect on this peak. In view of the crystallinity of cellulose being highly dependent on its HB network, this phenomenon also suggested that the crystallinity of the regenerated cellulose varies as a function of the anti-solvent. Our result differs from the result obtained through a molecular dynamics study.[16] From our point of view, the HBs of cellulose–anti-solvents were not taken into account in their calculation method. Without this, the analyzed targets are like

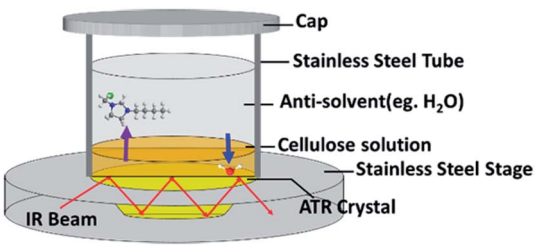

Fig. 1 Schematic illustration of the diffusion experimental configuration.

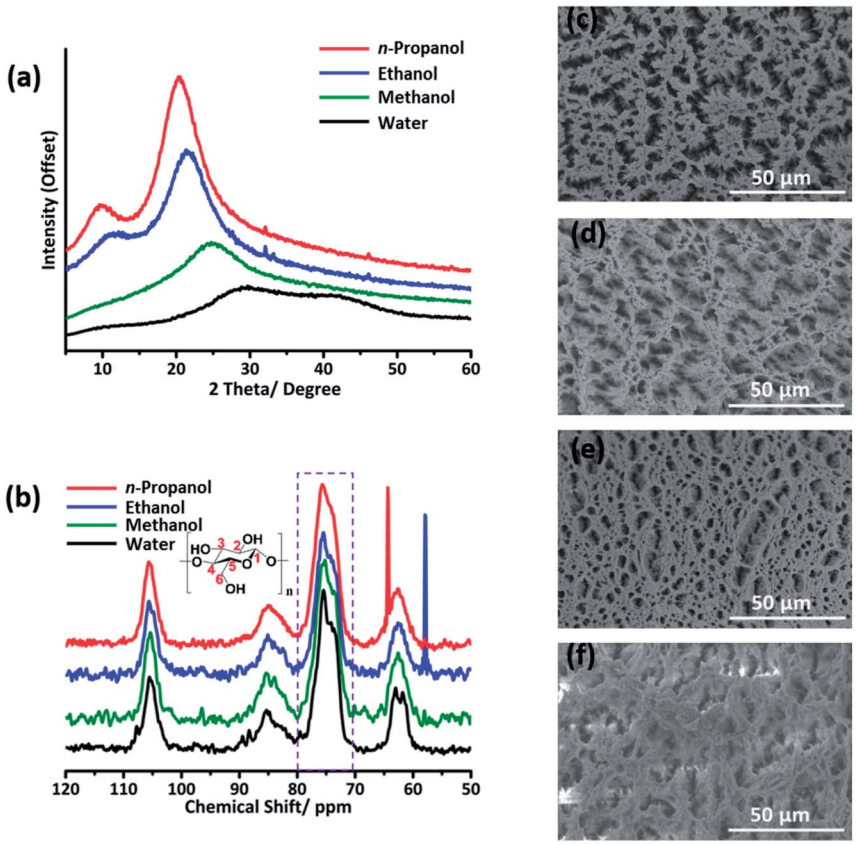

Fig. 2 Characterization of the regenerated cellulose gels by (a) XRD, (b) ^{13}C NMR and (c)–(f) SEM. The intensive peaks in the NMR spectra of the ethanol gel and *n*-propanol gel near 60 ppm are characteristic peaks of ethanol and *n*-propanol, respectively. The SEM images in (c), (d), (e) and (f) are for the cellulose aerogels regenerated by water, methanol, ethanol and *n*-propanol, respectively.

dried cellulose gels. During the drying process, cellulose may re-aggregate again. Moreover, the morphologies of the cellulose aerogels obtained by supercritical CO_2 drying are pictured by SEM (Fig. 2c–f). Evidently, fiber-like cellulose appeared in the ethanol/*n*-propanol regenerated aerogels. In contrast, a worm-like surface is presented for the water/methanol regenerated aerogels. This suggests that cellulose tends to rebuild highly crystallized cellulose in *n*-propanol, and amorphous cellulose in water. The cellulose gels regenerated by methanol/ethanol are transition states. Considering the relatively slow diffusion rates of *n*-propanol/ethanol, the variety of cellulose crystallinity is in all likelihood determined by the molecular diffusion rates of the anti-solvent molecules.

3.2 *In situ* monitoring of the diffusion processes by time dependent ATR-FTIR

To further explore the relationship between cellulose crystallinity and diffusion rates, time dependent ATR-FTIR was introduced to monitor the molecular diffusion processes *in situ* (Fig. 3a–d). At the very onset, only characteristic peaks of [Bmim]Cl showed in the IR spectra, since the cellulose solution film (~1000 μm) is thicker than the penetration depth of the evanescent wave (~1 μm at 1000 cm^{-1}).[20] As the anti-solvents diffused into the evanescent field, characteristic absorption peaks of the anti-solvents appeared, which increased as diffusion time prolonged and finally reached an equilibrium state. A longer time was observed from the beginning to the first detection signal of the anti-solvents in the sequence *n*-propanol (3354 s) > ethanol (1720 s) > methanol (688 s) > water (86 s). Additionally, the period of time to reach an equilibrium state increased in the same order (Fig. 3e). To date, it has been extensively accepted that free anions existing in ILs play a significant role in disrupting inter- and intra-hydrogen-bond networks of supramolecular cellulose.[8,24] Due to the high acidity of C2–H in the imidazolium ring, some researchers have pointed out that the imidazolium cation is also indispensable in dissolving cellulose.[25,26] The key to regenerating cellulose from ILs is disrupting the IL–cellulose HB network and rebuilding the cellulose–cellulose HB network. Sun[13] and co-workers measured the ^1H, ^{13}C and ^{15}N NMR spectra of [Bmim]OAc and [Bmim]OAc-CO_2, where CO_2 was used as an anti-solvent. Their results indicated that the reaction between [Bmim]OAc and CO_2 resulted in cellulose regeneration. The two peaks in the range 3200–3000 cm^{-1} both belong to C–H stretching in the imidazolium ring, where the wide peak at the lower wavenumber can be assigned to C2–H stretching for its strong acidic character and the higher wavenumber peak to C4/5H stretching.[27] Due to the formation of anti-solvent–imidazolium ring HBs, blue shifts of these two peaks occurred during

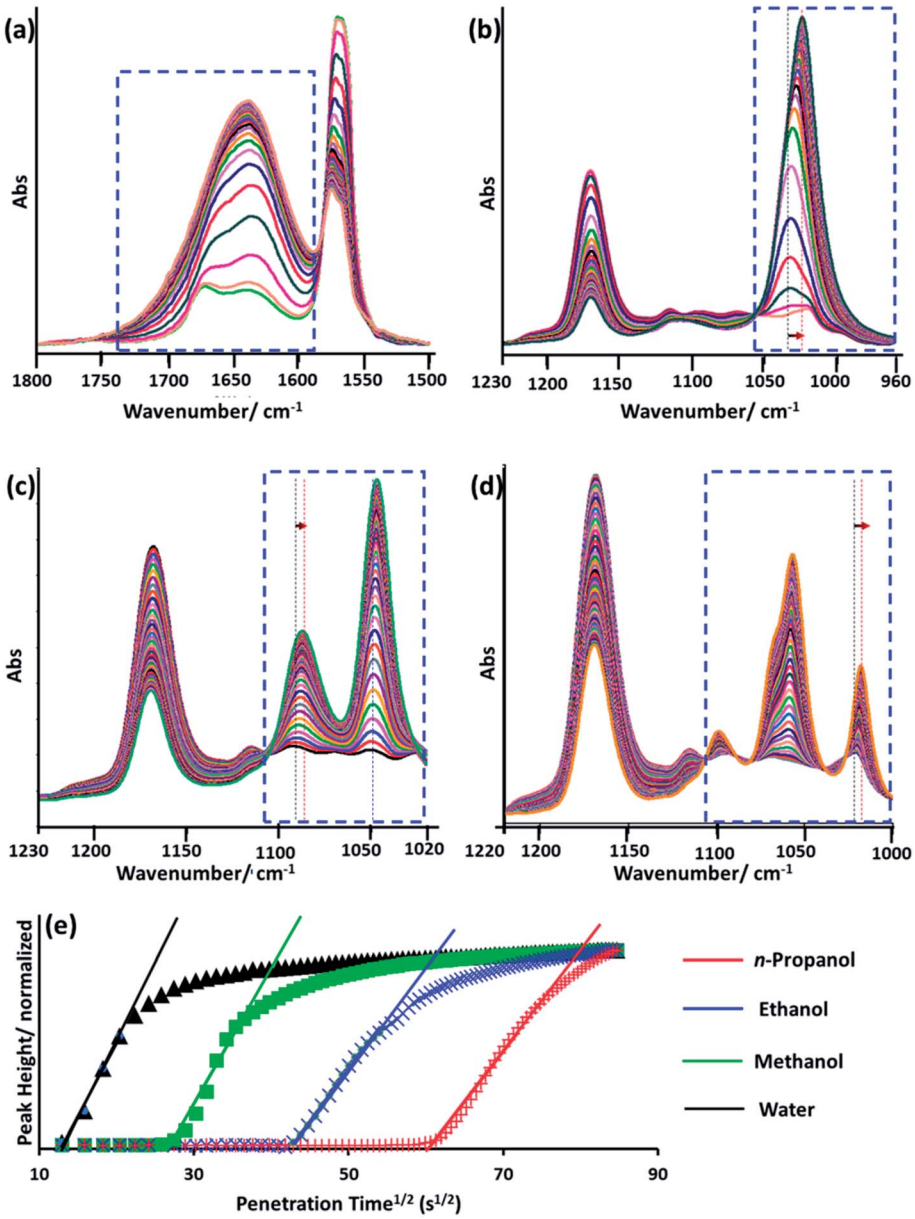

Fig. 3 ATR-FTIR spectra of the molecular diffusion processes: (a) water, (b) methanol, (c) ethanol, and (d) *n*-propanol, and diffusion curves of the four different anti-solvents (e). The peaks enclosed by blue dashed boxes are characteristic for the anti-solvents: (a) O–H bending of water, and (b)–(d) C–O stretching of methanol, ethanol and *n*-propanol, respectively. The interval time between two spectra is 86 seconds. The solid lines in (e) are fitting results according to the Fickian diffusion model when $A_t/A_e < 0.6$.

the diffusion processes (Fig. 4). Simultaneously, the C–O stretching peaks of the alcohols shifted to a lower wavenumber field (Fig. 3b–d). These peak shifts could be interpreted as a redistribution of charge densities through the formation of imidazolium cation–anti-solvent complexes rather than the simple direct C–H···O interaction.[28,29] Fig. 5 exhibits the supposed schematic charge transfer modes of the imidazolium cation–ethanol complex. The blue shift of the C–H stretching peaks of the alcohol and alkyl groups in the imidazolium ring confirmed the proposed charge transfer model (Fig. S1†). Moreover, the blue shift range of C2–H was much more than that of C4/5H, suggesting that C2–H interacts with the anti-solvent molecules more strongly than C4/5H. Such a conclusion was also confirmed by NMR.[30] When conducting proton exchange with deuterium, the exchange rates of all the ring protons increased greatly when adding NaOD, making the solution basic. Besides, deuterium exchange is faster for C2–H than for C4/5H. Meanwhile, larger blue shifts were also shown in the sequence *n*-propanol < ethanol < methanol < water. A larger range of blue shift means a stronger interaction between the imidazolium cation and anti-solvents. To quantify the diffusion processes, the diffusion coefficients of the anti-solvents were calculated based on the simplified Fickian diffusion equation (eqn (1)).[20]

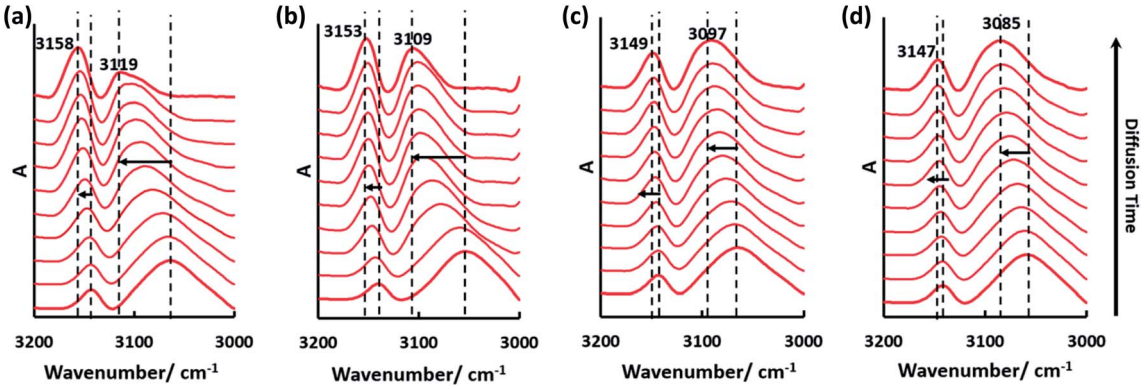

Fig. 4 The blue shift of peaks assigned to C–H stretching in the imidazolium ring during the molecular diffusion process of each anti-solvent: (a) water, (b) methanol, (c) ethanol and (d) *n*-propanol. The time interval of each spectrum is different from that of the four anti-solvents.

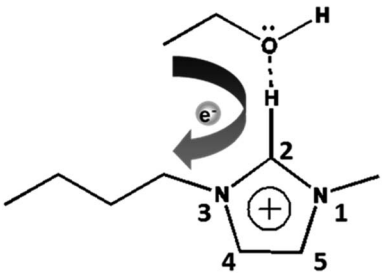

Fig. 5 Schematic model of charge transfer in the imidazolium cation–ethanol complex.

$$\frac{A_t}{A_e} = \frac{2}{L}\left(\frac{D}{\pi}\right)^{0.5} t^{0.5} \quad (1)$$

where A_t and A_e are the areas of the selected absorption peak of the anti-solvent at time t and at equilibrium, respectively. L is the thickness of the cellulose solution film. The equation is usable when $A_t/A_e < 0.6$.

The diffusion coefficient of each anti-solvent can be calculated based on eqn (1) (Table 1). As is shown, a fine linear relationship between A_t/A_e and $t^{0.5}$ appeared when $A_t/A_e < 0.6$ (Fig. 3e).

3.3 Semi quantitative analysis of the regenerated cellulose

Fig. 6a and b show the semi quantitative relationship between cellulose crystallinity and the diffusion coefficients of the anti-solvents. Both inter- and intra- cellulose chain HBs and cellulose–anti-solvent HBs may exist in the cellulose gel. The existence of cellulose–anti-solvent HBs has a negative effect on cellulose crystallinity, regenerating more amorphous cellulose. The inter- and intra- cellulose chain HB forms are mostly O(3)H···O(5), O(2)H···O(6) and O(6)···O(3).[31] Consequently, the peak shape at ~75 ppm, which is characteristic for C2,3,5 of cellulose, is influenced by HBs (Fig. 2b).[32] The relative sharpening of the peak at ~75.5 ppm may be caused by cellulose–anti-solvent HBs, decreasing the regenerated cellulose crystallinity. It is well known that the full width at half maximum (FWHM) of the diffraction peak is highly related to grain size. We calculated the relative peak height (RPH) of the peaks at ~75.5 and ~73.7 ppm after peak fitting using Origin 7.0 to semi quantify the crystallinity of the regenerated cellulose (Fig. S2†). Coupled with the ILs being solvated, the cellulose–cellulose HB network was rebuilt. With the ILs solvated slowly, the cellulose–cellulose HBs could rebuild finely, regenerating highly crystallized cellulose. Otherwise, cellulose–cellulose HBs were rebuilt as messy tangles of wires, regenerating amorphous cellulose. As a result,

Table 1 Diffusion coefficients, Taft and Kamlet scales and kinetic diameter of each anti-solvent

	Diffusion coefficient[a] (10^{-6} cm^2 s^{-1})	R^2	Taft and Kamlet scales (MPa$^{1/2}$)			Kinetic diameter (nm)
			α	β	π^*	
Water	27.39 ± 1.68	0.989 ± 0.010	1.17	0.47	1.09	0.26
Methanol	10.5 ± 1.51	0.990 ± 0.008	0.98	0.66	0.60	0.38
Ethanol	3.32 ± 0.82	0.995 ± 0.001	0.84	0.90	0.54	0.43
n-Propanol	2.03 ± 0.47	0.995 ± 0.003	0.84	0.90	0.54	0.47

[a] Taking the intensity of the absorption band into account, we selected 1740–1010, 1080–970, 1070–1010 and 990–970 cm^{-1} for water, methanol, ethanol and *n*-propanol, respectively. The area of each selected absorption band was corrected by the corresponding baseline points. Each anti-solvent was tested three times and the results are reproducable.

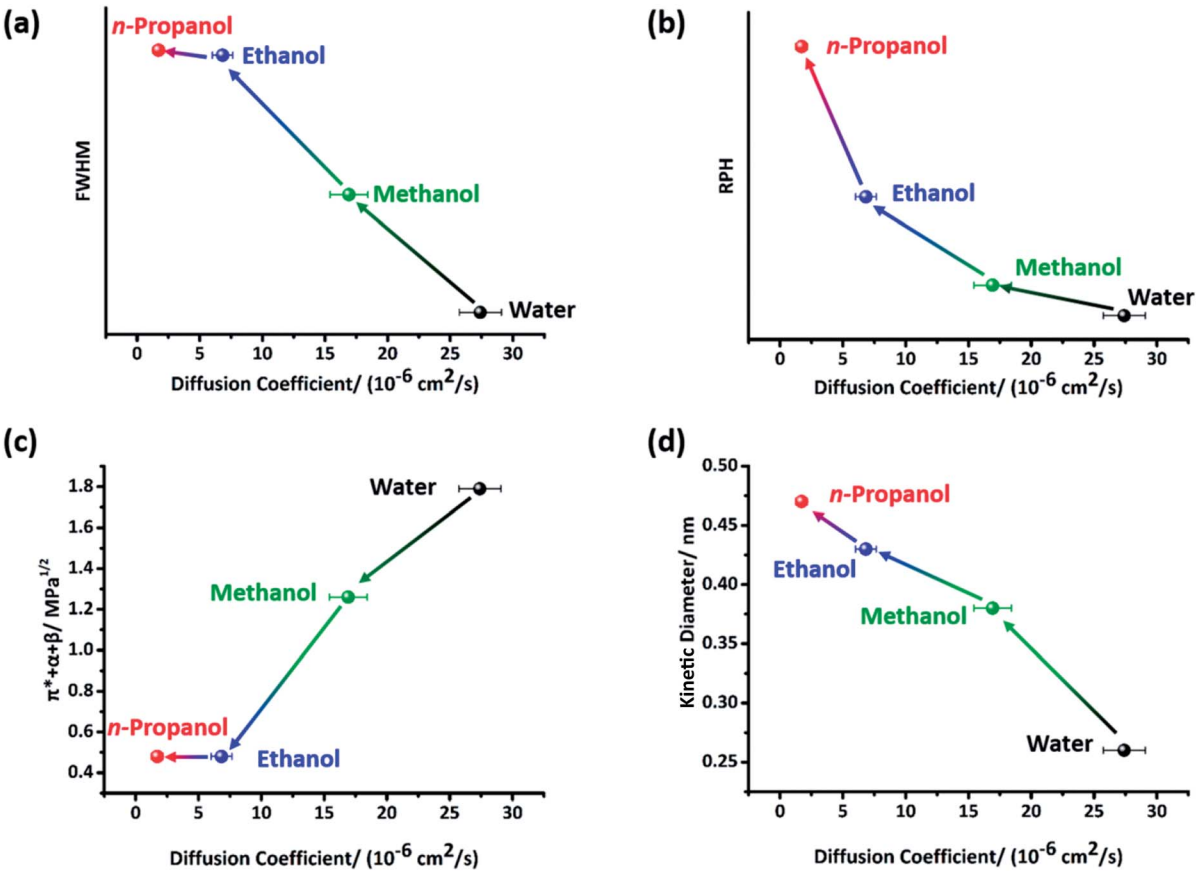

Fig. 6 The relationship between the diffusion coefficient of the anti-solvent and cellulose crystallinity: (a) cellulose crystallinity measured by the FWHM of the diffraction peak; (b) cellulose crystallinity measured by the RPH at ~75 ppm in NMR, and plots of the diffusion coefficients of the anti-solvents with respect to (c) the Taft and Kamlet scales ($\pi^* + \alpha + \beta$) and (d) the kinetic diameter of the anti-solvent molecules.

the cellulose crystallinity shows a negative correlation with respect to the diffusion coefficient.

3.4 Possible regeneration paths of the different anti-solvents

Taft and Kamlet scales have been extensively used to evaluate the interaction between molecules and ions.[20,33–35] Here, the sum of $\alpha + \beta + \pi^*$ was introduced to evaluate the interaction between the ILs and anti-solvents (Fig. 6c). Perplexingly, the $\pi^* + \alpha + \beta$ values of ethanol and *n*-propanol are identical, while the diffusion coefficients of them are unequal. We considered that the volume of the anti-solvent molecules also has a significant effect on the diffusion coefficients (Fig. 6d). Interestingly, the α and π^* values exhibit an opposite tendency to that of β, consistent with the varying trend in diffusion coefficient (Table 1). Since α measures HB donor acidity, this indicates that the anti-solvents tend to make chloride ions solvated prior to imidazolium cations. This result agrees with the conclusion drawn by T. Welton.[30,36] Welton and coworkers confirmed that all the imidazolium ring protons were hydrogen-bonded by halide anions by multinuclear NMR spectroscopy. Therefore, the imidazolium ring does not serve as a HB acceptor. In the following studies, they concluded that the water–anion complex existed as a 1 : 2 type, indicating an anion···HOH···anion structured complex. Furthermore, the peak shifts of C2–H (Fig. 4) were determined by not only β (HB acceptor basicity) but also π^* (molecular polarity). The relative values of α, β and π^* are $\alpha > \pi^* \gg \beta$ for water, $\alpha > \beta > \pi^*$ for methanol and $\beta > \alpha \gg \pi^*$ for ethanol/*n*-propanol. Since the main driving forces of the anti-solvents differ from each other, we assumed they have distinct regeneration paths. To be specific, water acted mostly as a HB donor rather than as a HB acceptor, making anions solvated more intensively. The interaction between imidazolium cations and cellulose was broken by solvation or electrostatic interaction. The interaction between IL ions and cellulose hydroxyl groups was broken in a relatively sharp path in water, resulting in amorphous cellulose. In contrast, ethanol/*n*-propanol more intensively interact with imidazolium cations. The interaction between cellulose and anion/imidazolium cations was broken mostly by solvation. With this relatively soft path, crystalized cellulose was regenerated. Methanol is a transition between water and ethanol/*n*-propanol.

4 Conclusion

Based on time dependent ATR-FTIR, we monitored *in situ* the diffusion processes of four anti-solvents into cellulose solution.

More crystallized cellulose was regenerated by anti-solvents with a lower diffusion coefficient. The interaction between imidazolium cations and anti-solvent molecules was evaluated through the blue shifts of C2–H stretching peaks. Besides, a charge transfer model for imidazolium cation–anti-solvent complexes was proposed according to the peak shifts. In addition, distinct cellulose regeneration paths for different anti-solvents were put forward through analysis of the interaction between ILs and anti-solvents using Taft and Kamlet scales.

Conflicts of interest

There are no conflicts to declare.

Acknowledgements

This research was supported by the National Natural Science Foundation of China (No. 31370556) and Beijing Municipality Science and Technology Planning Project (D161100002116001).

References

1 U.S. Energy Information Administration, 2017, https://www.eia.gov/renewable/data.php.
2 M. Jarvis, *Nature*, 2003, **426**, 611–612.
3 R. D. Rogers and K. L. Seddon, *Science*, 2003, **302**, 792–793.
4 H. Wang, G. Gurau and R. D. Rogers, *Chem. Soc. Rev.*, 2012, **41**, 1519–1537.
5 H. Abushammala, I. Krossing and M. Laborie, *Carbohydr. Polym.*, 2015, **134**, 609–616.
6 H. Zhang, J. Wu, J. Zhang and J. He, *Macromolecules*, 2005, **38**, 8272–8277.
7 Y. Li, X. Liu, S. Zhang, Y. Yao, X. Yao, J. L. Xu and X. Lu, *Phys. Chem. Chem. Phys.*, 2015, **17**, 17894–17905.
8 J. Moulthrop, R. Swatloski, G. Moyna and R. D. Rogers, *Chem. Commun.*, 2005, 1557–1559.
9 R. Swatloski, S. Spear, J. Holbrey and R. D. Rogers, *J. Am. Chem. Soc.*, 2002, **124**, 4974–4975.
10 R. Rinaldi, R. Palkovits and F. Schüth, *Angew. Chem., Int. Ed.*, 2008, **47**, 8047–8050.
11 F. Boissou, A. Mühlbauer, K. D. O. Vigier, L. Leclercq, W. Kunz, S. Marinkovic, B. Estrine, V. Nardello-Rataj and F. Jérôme, *Green Chem.*, 2014, **16**, 2463–2471.
12 D. Zhao, J. Huang, Y. Zhong, K. Li, L. Zhang and J. Cai, *Adv. Funct. Mater.*, 2016, **26**, 6279–6287.
13 X. Sun, Y. Chi and T. Mu, *Green Chem.*, 2014, **16**, 2736–2744.
14 Z. Liu, X. Sun, M. Hao, C. Huang, Z. Xue and T. Mu, *Carbohydr. Polym.*, 2015, **117**, 99–105.
15 B. Li, J. Asikkala, I. Filpponen and D. Argyropoulos, *Ind. Eng. Chem. Res.*, 2010, **49**, 2477–2484.
16 K. M. Gupta, Z. Hu and J. Jiang, *RSC Adv.*, 2013, **3**, 12794–12801.
17 Y. Mao, *Diffusion Competition Between Solvent and Nonsolvent During the Coagulation Process of Cellulose/Ammonia/Ammonium Thiocyanate Fiber Spinning System*, Wuhan University, Wuhan, 2005.
18 C. Liu, J. Cuculo and B. Smith, *J. Polym. Sci., Polym. Phys. Ed.*, 1990, **28**, 449–465.
19 H. P. Fink, P. Weigel, H. J. Purz and J. Ganster, *Prog. Polym. Sci.*, 2001, **26**, 1473–1524.
20 W. Guo, J. Chen, S. Sun and Q. Zhou, *J. Phys. Chem. C*, 2016, **120**, 7451–7456.
21 M. Karimi, A. A. Tashvigh, F. Asadia and F. Z. Ashtiani, *RSC Adv.*, 2016, **6**, 9013–9122.
22 A. A. Gabrienko, A. V. Ewing, A. M. Chibiryaev, A. M. Agafontsev, K. A. Dubkov and S. G. Kazarian, *Phys. Chem. Chem. Phys.*, 2016, **18**, 6465–6475.
23 Y. Wan, F. An, P. Zhou, Y. Li, Y. Liu, C. Lu and H. Chen, *Chem. Commun.*, 2017, 3595–3597.
24 R. C. Remsing, R. P. Swatloski, R. D. Rogers and G. Moyna, *Chem. Commun.*, 2006, 1271–1273.
25 B. Lu, A. Xu and J. Wang, *Green Chem.*, 2014, **16**, 1326–1335.
26 Y. Cao, R. Zhang, T. Cheng, J. Guo, M. Xian and H. Liu, *Appl. Microbiol. Biotechnol.*, 2017, **101**, 521–532.
27 C. Roth, S. Chatzipapadopoulos, D. Kerle, F. Friedriszik, M. Lutgens, S. Lochbrunner, O. Kuhn and R. Ludwig, *New J. Phys.*, 2012, **14**, 1–14.
28 L. Zhang, Y. Wang, Z. Xu and H. Li, *J. Phys. Chem. B*, 2009, **113**, 5978–5984.
29 N. Wang, Q. Zhang, F. Wu, Q. Li and Z. Yu, *J. Phys. Chem. B*, 2010, **114**, 8689–8700.
30 A. G. Avent, P. A. Chaloner, M. P. Day, K. R. Seddon and T. Welton, *J. Chem. Soc., Dalton Trans.*, 1994, 3405–3413.
31 B. Hinterstoisser, M. Åkerholm and L. Salmén, *Biomacromolecules*, 2003, **4**, 1232–1237.
32 R. H. Atalla and D. L. VanderHart, *Science*, 1984, **223**, 283–285.
33 R. W. Taft, M. H. Abraham, R. M. Doherty and M. J. Kamlet, *J. Am. Chem. Soc.*, 1985, **107**, 3105–3110.
34 A. Duereh, Y. Sato, R. L. Smith and H. Inomata, *ACS Sustainable Chem. Eng.*, 2015, **3**, 1881–1889.
35 K. Kuroda, H. Kunimura, Y. Fukaya, N. Nakamura and H. Ohno, *ACS Sustainable Chem. Eng.*, 2014, **2**, 2204–2210.
36 L. Cammarata, S. G. Kazarian, P. A. Salter and T. Welton, *Phys. Chem. Chem. Phys.*, 2001, **3**, 5192–5200.

